

A Low-power Color Mosaic Image Compressor Based on Optimal Combination of 1-D Discrete Wavelet Packet Transform and DPCM for Wireless Capsule Endoscopy

Kinde A. Fante, Basabi Bhaumik and Shouri Chatterjee

Department of Electrical Engineering, Indian Institute of Technology Delhi, Hauz Khas, New Delhi-110016, India

Keywords: Wireless Capsule Endoscopy, Discrete Wavelet Packet Transform, Mosaic Image Compressor, Low-power.

Abstract: A novel low-power endoscopic image compressor is designed that occupies small silicon chip area, gives a high compression rate and maintains acceptable image quality. By utilizing unique properties of human gastrointestinal tract images, computationally simple and elegant methods are employed. The employed methods are lifting scheme based two level 1-D discrete wavelet packet transform, uniform quantization, chrominance component sub-sampling, differential pulse code modulation and Golomb-Rice entropy encoder. All the modules are highly optimized from computational complexity, efficiency and memory requirement perspectives. The proposed algorithm requires neither demosaicking nor de-interleaving operations that require large memory and consume a significant amount of power. The proposed image compression scheme achieves a compression rate of 81.31 % with peak signal to noise ratio of 39.45 dB. The implementation of the algorithm in 130 nm standard CMOS process technology occupies a core area of 0.342 mm \times 0.342 mm. It consumes 48.4 μ W of power for encoding two color mosaic frames, with a resolution of 512 \times 512, per second. The proposed endoscopic image compression scheme gives a power consumption reduction of about two orders less than the realizations proposed in literature.

1 INTRODUCTION

Wireless Capsule Endoscope (WCE) (Idden et al., 2000) was introduced by Given Imaging Ltd in 2000. Since then it has been widely used to diagnose gastrointestinal abnormalities with minimal invasiveness. Its main electrical components are image sensor, RF transmitter, button battery and structured light source (LEDs) as shown in Figure.1. During the diagnostic procedure, the capsule is swallowed by the patient through the mouth. As it travels through the gastrointestinal (GI) tract with the aid of peristalsis, it captures high resolution color images of the GI tract wall which cannot be reached by the wired conventional endoscopy. The images are then transmitted by the wireless RF transmitter to a receiver worn round the patients waist for an average of eight hours before the battery runs out (Moglia et al., 2008). The capsule comes out of the digestive system along with the stool and it is discarded. The images are downloaded onto a workstation (PC) with appropriate image processing software to make a video. The diagnosis is done offline by Gastroenterologist.

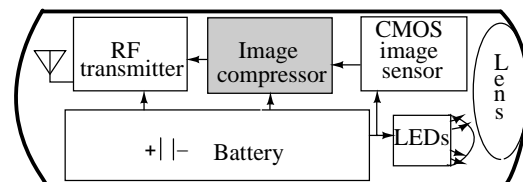


Figure 1: Block diagram of the wireless capsule endoscopy.

In order to reduce the power consumption of the RF transmitter without significant overhead, the image compressor inside WCE should have small chip area, low power consumption and maintain high image quality. Previous works on this topic were predominantly based on discrete cosine transform (DCT) and differential pulse code modulation (DPCM). The works in (Lin et al., 2006; Wahid et al., 2008; Dung et al., 2008; Lin and Dung, 2011; Chen et al., 2009; Turcza and Duplaga, 2011; Xie et al., 2007; Turcza and Duplaga, 2013) have used block-based DCT in order to encode endoscopic color mosaic images. These block-based transforms require huge memory to buffer data when they work with image sensor

that sends the pixel values in raster scan fashion. The DPCM based algorithms were proposed for both mosaic and full color image formats. The works proposed for mosaic image compression (Xie et al., 2006; Cheng et al., 2010) have used JPEG-LS algorithm which requires to store at least one row of the previously encoded pixels for prediction. The context variables also require 1.9KB of memory (Cheng et al., 2010). The DPCM based algorithms which were proposed for full color image compression (Khan and Wahid, 2011b; Khan and Wahid, 2011a) are simple. However, these algorithms require the implementation of the demosaicing algorithms inside the image sensor which consumes considerable amount of power and need memory. Memory consumes high power and occupies large silicon area which increases the overhead of the image compressor. Demosaicing the mosaic image increases its size by threefold which reduces the effective compression rate by the same amount. Despite its success in many applications, wavelet based image compression algorithm has not been explored for WCE application to the best of the authors' knowledge. In this work we present the study and design of wavelet based mosaic image compression algorithm which does not require huge memory buffer and is computationally simple.

The proposed image compressor combines multiple methods which are computationally simple to achieve high compression efficiency. These methods are: lifting scheme based discrete wavelet packet transform (DWPT), DPCM, uniform quantization, sub-sampling and Golomb-Rice encoding. The novelty of this work lies in modifying the wavelet filter coefficients to utilize the unique properties of human GI tract images. It also combines DWPT with DPCM, uniform quantization and sub-sampling optimally to achieve its target. We have experimentally determined the optimal combinations of the sub-sampling and uniform quantization parameters that can achieve the desired performance for WCE application. The final contribution of this work is optimization of Golomb-Rice encoder from memory requirement and efficiency perspective. The Golomb-Rice encoder parameter, k , is determined dynamically from local image properties using only four contexts in order to reduce the memory requirement and still maintain its adaptability property. The context variables require only 34 bytes of memory. We get a memory reduction of about 1.866 KB as compared to the method proposed in (Xie et al., 2006; Cheng et al., 2010). The image compressor can elongate the lifetime of the WCE significantly so that it can cover the whole GI tract.

The rest of the paper is organized as follows. The

detailed discussion of the proposed algorithm is given in section 2. The performance evaluation of the algorithm is presented in section 3. The hardware implementation is discussed in the section 4. The conclusion is given in the section 5.

2 ANALYSIS OF SUITABLE METHODS FOR EFFICIENT COMPRESSION OF WCE IMAGE

Mosaic image is captured using color filter arrays (CFA) (Bayer, 1976) shown in Figure 2 (a). The spectral bands are interleaved in mosaic image. The pixel values have high frequency content in its neighborhood. Hence, conventional image compression methods fails to give high compression efficiency for mosaic images. In the following sections we will show how computationally simple methods can be optimally combined to achieve high compression efficiency for WCE mosaic image.

2.1 Analysis of Color Mosaic Image Using Wavelet

Consider a pair of rows of color mosaic image which has six elements per row as shown in table 1, where the spectral band samples are given as R (red), G (green) and B (blue). Let's apply 1-D DWPT on this image using 5-3 integer wavelet (Angelopoulou et al., 2007) with lifting scheme (Sweldens, 1995). We use the horizontal filtering operation as shown in Figure 3.

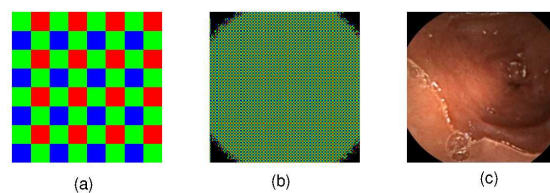


Figure 2: The Bayer arrangement of color filters on the pixel array of an image sensor (a), mosaic WCE image (b) and typical WCE full color image (c).

Table 1: Two rows of color mosaic image.

$G_{0,0}$	$R_{0,1}$	$G_{0,2}$	$R_{0,3}$	$G_{0,4}$	$R_{0,5}$
$B_{1,0}$	$G_{1,1}$	$B_{1,2}$	$G_{1,3}$	$B_{1,4}$	$G_{1,5}$

If we directly apply the lifting scheme 1-D DWT on the color mosaic image which is given in table 1, we will get the following outputs. For the first row, the

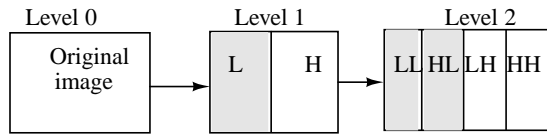


Figure 3: Diagrammatic representation of dyadic decomposition for two decomposition levels using horizontal filtering.

high-pass filter (H_R) and low-pass filter (L_G) outputs after horizontal filtering are given by:

$$H_R[2i, 2j + 1] = R_{2i, 2j+1} - \lfloor \frac{G_{2i, 2j} + G_{2i, 2j+2}}{2} \rfloor \quad (1)$$

$$L_G[2i, 2j] = G_{2i, 2j} + \lfloor \frac{H_R[2i, 2j-1] + H_R[2i, 2j+1] + 2}{4} \rfloor \quad (2)$$

where i and j are row and column indexes of the image array. Similarly, for the second row of image given in table 1, the high-pass filter (H_G) and low-pass filter (L_B) outputs after horizontal filtering are given by:

$$H_G[2i + 1, 2j + 1] = G_{2i+1, 2j+1} - \lfloor \frac{B_{2i+1, 2j} + B_{2i+1, 2j+2}}{2} \rfloor \quad (3)$$

$$L_B[2i + 1, 2j] = B_{2i+1, 2j} + \lfloor \frac{H_G[2i + 1, 2j-1] + H_G[2i + 1, 2j+1] + 2}{4} \rfloor \quad (4)$$

Our simulation result on 120 endoscopic images taken from Gastrolab (Gastrolab, 2014) shows that the smoothness of the low-pass filter outputs (L_G and L_B) are worse than the G and B color channels when they are de-interleaved. For this reason, the low-pass filtering operation of (2) is modified as:

$$L_G[2i, 2j] = G_{2i, 2j} \quad (5)$$

Similarly, the low-pass filtering operation given in (4) is modified as:

$$L_B[2i + 1, 2j] = B_{2i+1, 2j} \quad (6)$$

Figure 4 shows the statistical measurements (entropy and standard deviation) of the decomposed mosaic image given in Figure 2(b) using 1-D DWPT when the low-pass filtering operation is done using the original equations (2) and (4), and the modified equations (5) and (6). The modification of the low-pass filtering operation gives two advantages: It reduces computational resources and improves the compression efficiency.

We observed from Figure 4 that the average statistical measurements of the subbands of the decomposed color mosaic image do not show significant change after second level decomposition. Therefore,

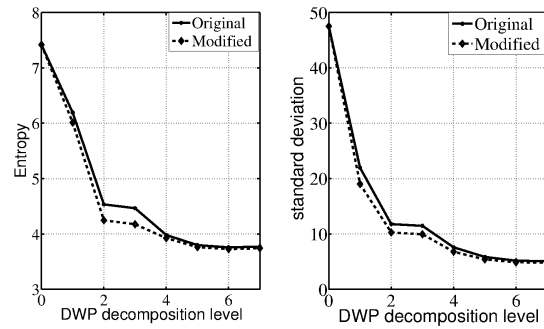


Figure 4: Average entropy (left) and standard deviation (right) of 120 endoscopic images at different wavelet packet decomposition level.

the level of decomposition is limited to two in order to save computational resources.

After the second level DWP decomposition, three quarter of the subbands of the mosaic image are low-pass signals. Figure 5 shows that the histogram of detail subbands (HH and HL subbands) of the second level DWPT is narrow and the values are small, near zero with high probability. The LH subband shows narrower histogram than the LL subband. The subbands which have narrow histogram can be efficiently encoded using computationally simple image compression techniques such as DPCM.

The 2-D decomposition of color mosaic images using Mallat wavelet packet was discussed in (Zhang and Wu, 2004). The authors have shown the simultaneous de-correlation of spectral and spatial redundancies of mosaic image using the convolution based 5-3 integer wavelet. The convolution based wavelet decomposition has higher computational complexity as compared to the lifting scheme (Sweldens, 1995). The 2-D decomposition of the mosaic image enables to de-correlate the image in both the vertical and horizontal direction. Hence, it gives higher compression efficiency than its 1-D counterpart. However, the 2-D based operation requires huge memory to buffer data during computation especially when the image compressor works with image sensor which sends pixel values in raster-scan fashion. Since memory occupies large area and consumes high power we use the 1-D based decomposition for this area and power constrained application. In the subsequent sections we show that 1-D DWP decomposition of mosaic endoscopic image can be optimally combined with DPCM, uniform quantization and sub-sampling to achieve a high compression rate.

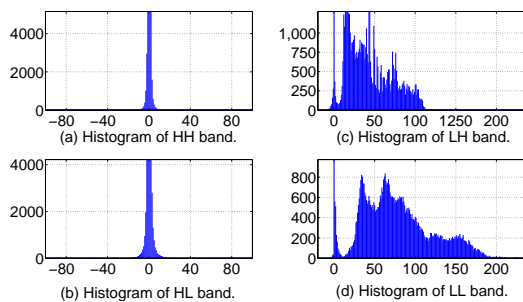


Figure 5: Histogram of the subbands of mosaic image shown in Figure 2 (b) after second level wavelet packet decomposition.

2.2 Uniform Quantization and Sub-sampling

The detail subbands of the first level DWP decomposition of color mosaic image, which are given by (1) and (3), represent the chrominance component of a color image. These subbands are the color difference images (R-G and G-B) which are low-pass signals because of the high correlation between RGB color channels. Human GI tract has a reddish color. There is a little sharp color transition in human GI tract. The absence of sharp color transitions in human GI tract enables to sub-sample chrominance components of the GI tract images without much loss of information. After first level discrete wavelet decomposition of color mosaic image, the high frequency wavelet subbands (H_R and H_G) are down-sampled to reduce the size of image. For example, image is down-sampled by two by removing every other column from the image. Sub-sampling is a computationally simple and efficient image compression technique.

In addition to DWPT, the high frequency content of the mosaic image can be reduced using a computationally simple way of low-pass filtering operation (Pattanaik et al., 2006) which uses quantization. The quantization operation can be done using only addition and shift operation if the quantizer is in the form of power-of-two. It has very simple hardware realization. For a given pixel value P and a quantizer value q , where q is positive integer, the quantized pixel value P_q is given by:

$$P_q = \left\lfloor \frac{P}{q} + 0.5 \right\rfloor \quad (7)$$

From the statistics point of view it is obvious that the standard deviation of the a set of pixel values is reduced by $\frac{1}{q}$ when the set is uniformly quantized using quantizer value q . Whereas the maximum error introduced when the values are dequantized is limited to $\frac{q}{2}$. If a set of pixels have low standard deviation, then it

will have higher spatial correlation which is important for efficient compression. Note that the uniform quantization supports the DWP decomposition in reducing the high frequency components of mosaic image. As shown in table 2, the proper combination of quantizer and sub-sampler gives optimal performance in terms of compression rate and image quality. We have chosen quantizer value of four and the down-sampling factor of four as optimal parameters.

2.3 Differential Pulse Code Modulation (DPCM)

After second level DWP decomposition of color mosaic image, two subbands (LL and LH) have large values and the other two subbands (HH and HL) have small values near to zero as shown in Figure 5. The small values can be efficiently encoded using Golomb-Rice entropy encoder. We use DPCM scheme subband-wise to remove spatial redundancy in the LH and LL subbands. In DPCM scheme, the current pixel, X , is estimated from previously encoded neighborhood pixels and then the estimated pixel value, X_p , is subtracted from current pixel value to get prediction error, $dX = X - X_p$. If the prediction accuracy is high, then the prediction error will be small and can be efficiently encoded. In baseline lossless JPEG standard (JPEG, 1998), up to six different prediction modes are recommended. We have chosen the simplest and static prediction mode which estimates the current pixel from a previously encoded pixel in the same row and same subband in order to reduce the computational complexity and to avoid the memory required to buffer one row of previously encoded pixels. As shown in Figure 6 the prediction error of LL and LH subbands have small values which can be efficiently encoded using computationally simple entropy encoding techniques such as Golomb-Rice encoder as shown in the next section.

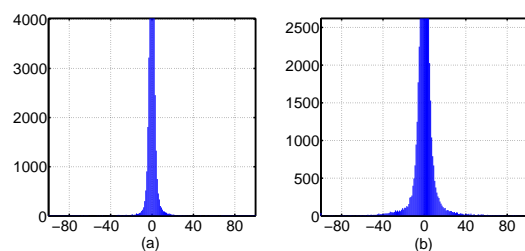


Figure 6: Histogram of the DPCM prediction error of LH (a) and LL (b) subbands for the mosaic image shown in Figure 2(b).

2.4 Locally Adaptive Optimized Golomb-Rice Encoder

After second level DWPT decomposition of mosaic image, the detail subbands (HH and HL subbands) have two-sided laplacian distribution around zero as shown in Figure 5 (a) and (b). Similarly, the prediction error of the DPCM scheme applied on approximate subbands (LL and LH subbands) have a two-sided laplacian distribution around zero as shown in Figure 6. Golomb-Rice (GR) coding (Golomb, 1966; Rice, 1991) is simple and efficient for encoding positive integers that form two-sided geometric distribution around zero (Gallager and Voorhi, 1975) and has been implemented in baseline JPEG-LS standard (JPEG, 1998). In JPEG-LS two modes of encoding are employed: regular mode and run-length encoding mode. Experiments show that the runs are too short in endoscopic image except at the corners. Hence, we do not use the run-length coding mode to save silicon area and power consumption.

In the regular mode of JPEG-LS encoding, the Golomb-Rice encoder parameter k , is determined from the global image statistics using 365 contexts. The context variable requires a memory of size 1.9 KB (Chen et al., 2009) which is potentially expensive for power and area constrained device like WCE. Non-adaptive parameter k based Golomb-Rice encoding was used in (Khan and Wahid, 2011b). The fixed parameter based Golomb-Rice encoding gives lower compression rate than the adaptive one.

We have modified the regular mode of JPEG-LS encoder in order to reduce the memory requirement. In our case, we have used only a single context to determine the parameter k for each subbands. By using single context for each subband, the Golomb-Rice parameter, k , can adapt to local statistics of the pixel values. We use two registers in order to store the accumulated values and to count the number of contexts encountered so far for each of the subbands. By using single context in Golomb-Rice encoder we have simplified the encoding process and still maintain its adaptability property. Totally, we have used four contexts, one for each subband in order to make the parameter adaptation intra-subband. Each subband is encoded separately because of the difference in their statistical properties. The maximum number of previously encoded values to be stored for the parameter k estimation is determined using a constant N_0 . This value is determined experimentally for the optimal hardware cost and compression efficiency and it is found to be 8 (64 in JPEG-LS). The context variables require only 34 bytes of memory which is very small.

2.5 The Proposed Image Compression Algorithm

The block diagram of the proposed image compressor is depicted in Figure 7. Due to the square shape of image sensor and circular shape of the lens inside endoscopic capsule, the corner region pixels have no important information as shown in Figure 2(b). This regions can be cropped without any loss of information. The corner pixels are cropped using the algorithm proposed in (Khan and Wahid, 2011a). The mosaic image pixel values are quantized to increase the spatial correlation in the neighborhood pixels as described in section 2.2. The the first level DWPT is applied on the quantized pixel values as described in section 2.1. The chrominance (H subband) components of the first level wavelet decomposition of the mosaic image is down-sampled to reduce the image size. Then L subband of the first level wavelet decomposition and the down-sampled H subband are further decomposed into four subbands (LL, LH, HH and HL) by applying second level wavelet decomposition. DPCM is applied on the LL and LH subbands of the second level DWPT as given in section 2.3. Finally, locally adaptive Golomb-Rice encoder is used as an entropy encoder as described in section 2.4. The decoding operation is the inverse of the encoding process.

3 PERFORMANCE EVALUATION

The performance of image compression algorithm is evaluated using compression rate (CR) and given by:

$$CR = \left(1 - \frac{\text{Image size after compression}}{\text{Image size before compression}}\right) \times 100 \% \quad (8)$$

The proposed image compression algorithm is lossy due to the quantization and sub-sampling operations. The quality of the decompressed image is evaluated using peak signal to noise ratio (PSNR)(Korhonen and Junyong, 2012) which is given by:

$$PSNR = 10 \log_{10} \left(\frac{255^2}{\frac{1}{MN} \sum_{x=1}^M \sum_{y=1}^N (f(x,y) - \tilde{f}(x,y))^2} \right) \quad (9)$$

where M and N are width and height of the original image $f(x, y)$ and the noisy image $\tilde{f}(x, y)$, x and y are coordinates of the pixel. All the experiments in this work are done using 120 endoscopic images obtained from Gastrolab (Gastrolab, 2014). The test images include the images of the whole GI tract, from esophagus to colon. Therefore, we believe that these images are a good representative of the whole human digestive system images. The images are originally available in RGB full color format. For our experiment, we

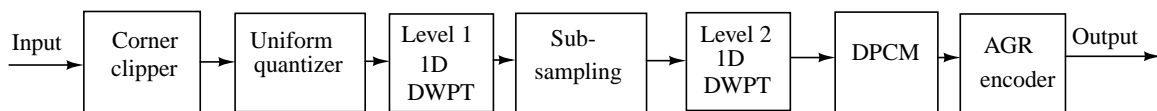


Figure 7: Block diagram of the proposed endoscopic image compressor.

Table 2: The performance of the proposed image compression algorithm for different parameters.

Parameters		CR (%)	PSNR (dB)
Quantizer	H subband sub-sampling factor		
1	-	55.02	∞
2	-	65.49	51.3719
4	-	73.57	46.6142
8	-	78.35	41.0004
-	2	63.22	46.2585
-	4	68.05	41.2555
-	8	71.01	36.75
4	2	78.59	40.6736
4	4	81.31	39.4471
4	8	82.95	36.6333

have converted the full color images into color mosaic images using matlab. For visual comparison (subjective image quality assessment) both original mosaic images and the decompressed images are converted to full color images using a demosaicing algorithm (Getreuer, 2011). The performance of the proposed image compression algorithm is shown in table 2.

As shown in Table 2, the lossless mode of the proposed image compressor gives a compression rate of 55.02 %. The nearly-lossless and lossy versions of the algorithm give up to 82.95 % compression rate. This implies that the proposed image compressor (quantizer=4 and H subband down-sampling by 4) reduces the size of image by an average factor of 5.5. It has an average peak signal to noise ratio (PSNR) of 39.45 dB which is greater than minimum PSNR (35dB)(Istepanian et al., 2008; Cosman et al., 1994) required for accurate diagnosis of medical images.

4 HARDWARE REALIZATION

The block diagram of the proposed image compressor is given in Figure 8. The image compressor takes 8-bit pixel value from image sensor at every rising edge of clock (or CLK) signal. The image sensor also sends row (HSYNC) and frame synchronisation (VSYNC) to indicate the end of a row and frame respectively. The image compressor requires computationally simple methods such as adders, shift registers, counters etc. The lifting scheme based 1-D wavelet decom-

position of mosaic image is done modifying the architecture proposed in (Angelopoulou et al., 2007). In the modified architecture the first level wavelet decomposition is done according to the equations given in (5) and (6). The Golomb-Rice encoder generates a codeword (CW) of length 32 and codeword index (CWI). The codeword index holds the index to MSB of the generated code in the 32-bit CW. No memory buffer is used in the implementation, only few registers are employed.

The proposed endoscopic image compression algorithm (with quantizer $q=4$ and sub-sampling the high frequency subband of first level wavelet decomposition by 4) has been implemented in both MATLAB and VHDL for verification. The image compressor was implemented in MATLAB scripts and VHDL. The image decompressor is implemented only in MATLAB. After the functionality of the algorithm is verified using 120 endoscopic images, the VHDL code is synthesized and mapped to UMC 130 nm Faraday high speed (HS) library using Synopsys Design Compiler. After post-synthesis functional verification of the algorithm is done using QuestaSim and MATLAB, the layout is generated using Cadence Soc Encounter place and route tool. The layout view of the core of the chip is shown in Figure.9. The proposed image compression algorithm has core size of 0.342 mm x 0.342 mm. The power consumption of the synthesized design is estimated using Synopsys PrimeTime PX. The mean power consumption of the image compressor is $48.4\mu W$ when operating at two frames per second (fps) for encoding 512x512 color mosaic image. The operating voltage is 1.2V.

The performance comparison of the proposed algorithm with other existing works is given in table 3. We compare our proposed image compressor with one algorithm which is based on JPEG-LS (Xie et al., 2006) and two algorithms which are based on DCT (Lin and Dung, 2011; Turcza and Duplaga, 2013). All the competing algorithms included in the table

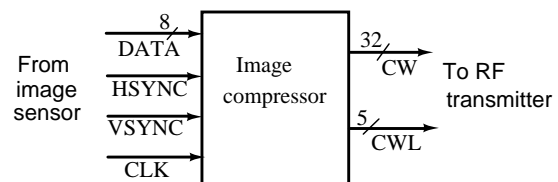


Figure 8: Block diagram of the proposed image compressor implementation.

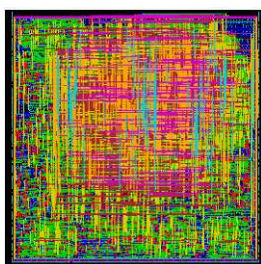


Figure 9: Layout view of the core of the proposed image compressor implementation.

Table 3: The comparison results with previous works.

	(Xie et al., 2006)	(Lin et al., 2011)	(Turcza et al., 2013)	This work
Methods	JPEG-LS	DCT	DCT	DWPT
Compression Rate (%)	72.7	82.0	91.2	81.31
Overall PSNR (dB)	46.8	36.2	35.7	39.5
Technology	ASIC 0.18 μm	ASIC 0.18 μm	FPGA 65nm	ASIC 0.13 μm
Core size (μm^2)	90K gates	318K	-	117K
Memory (byte)	93.81K	YES	10.5K	0
Power consumption (mW)	1.55 (0.28 fps)	9.17 (2 fps)	7 (7 fps)	0.048 (2 fps)
Supply Voltage(V)	1.8	1.8	1.2	1.2

were tested with similar images of 512 x 512 resolution. The proposed image compression algorithm doesn't require memory and consumes about two orders of less power than other algorithms as shown in table 3. Our algorithm has also the lowest chip area as compared to other works. The proposed algorithm outperforms work in (Xie et al., 2006) in terms of compression rate. It gives a comparable compression rate with a work in (Lin and Dung, 2011) but has also higher image quality. It achieves lower compression rate than the work in (Turcza and Duplaga, 2013). However, the work in (Turcza and Duplaga, 2013) needs about 10.5 KB of memory which consumes high power and occupies large silicon area. Generally, DCT based compression algorithms introduce blocking effect due to the quantization of DCT coefficients. The proposed algorithm doesn't introduce blocking effect which is indispensable for precise diagnosis of medical images. As shown in Figure.10, the proposed endoscopic image compression algorithm doesn't introduce noticeable artifacts in the reconstructed image. The proposed endoscopic image compression algorithm meets all the criterion to be a serious candidate for WCE.

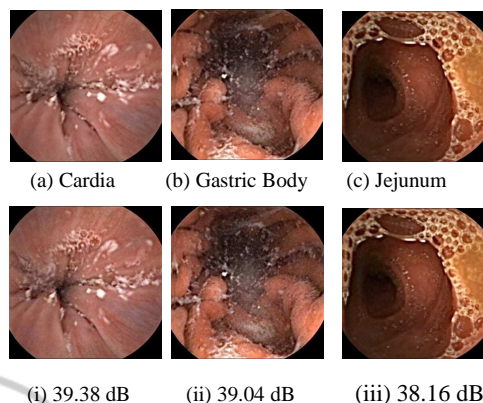


Figure 10: Three endoscopic images out of 120 test images that we have employed in the experimentation. The original (top) and reconstructed images (bottom) with PSNR value.

5 CONCLUSION

In this paper, we have presented a low-power image compression algorithm for WCE application. The algorithm uses optimal combination of methods which are computationally simple. Utilizing the combination of computationally simple methods we have achieved a compression rate of 81.3 %. The compressed image has a high image quality (39.5 dB) which is greater than the minimum PSNR (35 dB)(Istepanian et al., 2008; Cosman et al., 1994) required for accurate medical image diagnosis. The proposed image compression algorithm has relatively high compression rate, small chip area, low power consumption and high image quality which makes it a good candidate for WCE application.

The future work includes the design of the whole capsule system and testing its performance in real-world. The impact of the distortion introduced due to the image compressor on automatic disease detection algorithms will be studied.

REFERENCES

Angelopoulou, M. E., Cheung, P. Y. K., Masselos, K., and Andreopoulos, Y. (2007). Implementation and comparison of the 5/3 lifting 2d discrete wavelet transform computation schedules on fpgas. *Springer, Journal of VLSI Signal Processing*.

Bayer, B. E. (1976). Color imaging array.

Chen, X., X., Zhang, L., Li, X., Qi, N., Jiang, H., and Wang, Z. (2009). A wireless capsule endoscope system with low-power controlling and processing asic. *IEEE Transactions on, Biomedical Circuits and Systems*, 3(1):11–22.

- Cheng, C., Liu, Z., Hu, C., and Meng, M. (2010). A novel wireless capsule endoscope with jpeg compression engine. In *2010 IEEE International Conference on Automation and Logistics (ICAL)*, pages 553–558.
- Cosman, P., Gray, R., and Olshen, R. (1994). Evaluating quality of compressed medical images: Snr, subjective rating, and diagnostic accuracy. *Proceedings of the IEEE*, 82(6):919–932.
- Dung, L., Wu, Y., Lai, H., and Weng, P. (2008). A modified h.264 intra-frame video encoder for capsule endoscope. In *BioCAS 2008, IEEE Biomedical Circuits and Systems Conference*, pages 61–64.
- Gallager, R. and Voorhi, D. V. (1975). Optimal source codes for geometrically distributed integer alphabets (corresp.). *IEEE Transactions on Information Theory*, 21(2):228–230.
- Gastrolab (2014). <http://gastrolab.net/> (Online available), last visited 2014.
- Getreuer, P. (2011). Color demosaicing with contour stencils. In *17th International Conference on Digital Signal Processing (DSP)*, pages 1–6.
- Golomb, S. (1966). Run-length encodings (corresp.). *IEEE Transactions on Information Theory*, 12(3):399–401.
- Idden, G., Meron, G., Glukhovskiy, A., and Swain, P. (2000). Wireless capsule endoscopy. *Nature*.
- Istefanian, R., Philip, N., Martini, M., Amso, N., and Shorvon, P. (2008). Subjective and objective quality assessment in wireless teleultrasonography imaging. In *EMBS 2008, 30th Annual International Conference of the IEEE Engineering in Medicine and Biology Society*.
- JPEG (1998). Lossless and near-lossless compression of continuous-tone still images baseline. *JPEG-LS, T.87*.
- Khan, T. and Wahid, K. (2011a). Low power and low complexity compressor for video capsule endoscopy. *IEEE Transactions on Circuits and Systems for Video Technology*, 21(10):1534–1546.
- Khan, T. and Wahid, K. (2011b). Subsample-based image compression for capsule endoscopy. *Journal of Real-Time Image Processing*, 8(1):5–19.
- Korhonen, J. and Junyong, Y. (2012). Peak signal-to-noise ratio revisited: Is simple beautiful? In *Fourth International Workshop on Quality of Multimedia Experience (QoMEX)*.
- Lin, M. and Dung, L. (2011). A subsample-based low-power image compressor for capsule gastrointestinal endoscopy. *EURASIP Journal on Advances in Signal Processing*, 2011.
- Lin, M., Dung, L., and Weng, P. (2006). An ultra-low-power image compressor for capsule endoscope. *BioMedical Engineering OnLine*, 5(14).
- Moglia, A., Menciassi, A., and Dario, P. (2008). Recent patents on wireless capsule endoscopy. *Recent Patents on Biomedical Engineering*.
- Pattanaik, S., Mahapatra, K., and Panda, G. (2006). A novel lossless image compression algorithm using arithmetic modulo operation. In *IEEE Conference on Cybernetics and Intelligent Systems*, pages 1–5.
- Rice, R. F. (1991). Some practical universal noiseless coding techniques - part iii. *Tech. Rep. JPL-91-3, Jet Propulsion Laboratory*.
- Sweldens, W. (1995). Lifting scheme: A new philosophy in biorthogonal wavelet constructions. In *proc. SPIE*, volume 2569.
- Turcza, P. and Duplaga, M. (2011). Low power fpga-based image processing core for wireless capsule endoscopy. *Sensors and Actuators A: Physical*, 172(2):552–560.
- Turcza, P. and Duplaga, M. (2013). Hardware-efficient low-power image processing system for wireless capsule endoscopy. *IEEE Journal of Biomedical and Health Informatics*, 17(6):1046–1056.
- Wahid, K., Ko, S., and Teng, D. (2008). Efficient hardware implementation of an image compressor for wireless capsule endoscopy applications. In *IJCNN'08, IEEE International Joint Conference on Neural Networks (IEEE World Congress on Computational Intelligence)*.
- Xie, X., Li, G., Chen, X., Li, X., and Wang, Z. (2006). A low-power digital ic design inside the wireless endoscopic capsule. *IEEE Journal of Solid-State Circuits*, 41(11):2390–2400.
- Xie, X., Li, G., and Wang, Z. (2007). A near-lossless image compression algorithm suitable for hardware design in wireless endoscopy system. *EURASIP Journal on Advances in Signal Processing*.
- Zhang, N. and Wu, X. (2004). Lossless compression of color mosaic images. In *ICIP '04, International Conference on Image Processing*.